



HAL
open science

Evaluation of tsunami inundation in the plain of Martil (north Morocco): Comparison of four inundation estimation methods

Elise Basquin, Apolline El Baz, Jacques Sainte-Marie, Alain Rabaute, Maud Thomas, Sara Lafuerza, Abdelmounim El M'Rini, Denis Mercier, Elia D'acremont, Marie-Odile Bristeau, et al.

► To cite this version:

Elise Basquin, Apolline El Baz, Jacques Sainte-Marie, Alain Rabaute, Maud Thomas, et al.. Evaluation of tsunami inundation in the plain of Martil (north Morocco): Comparison of four inundation estimation methods. *Natural Hazards Research*, 2023, 10.1016/j.nhres.2023.06.002 . hal-04134599

HAL Id: hal-04134599

<https://hal.science/hal-04134599>

Submitted on 3 Nov 2023

HAL is a multi-disciplinary open access archive for the deposit and dissemination of scientific research documents, whether they are published or not. The documents may come from teaching and research institutions in France or abroad, or from public or private research centers.

L'archive ouverte pluridisciplinaire **HAL**, est destinée au dépôt et à la diffusion de documents scientifiques de niveau recherche, publiés ou non, émanant des établissements d'enseignement et de recherche français ou étrangers, des laboratoires publics ou privés.



Distributed under a Creative Commons Attribution - NonCommercial - NoDerivatives 4.0 International License



Evaluation of tsunami inundation in the plain of Martil (north Morocco): Comparison of four inundation estimation methods

Elise Basquin^{a,b,c,*}, Apolline El Baz^d, Jacques Sainte-Marie^d, Alain Rabaute^e, Maud Thomas^f, Sara Lafuerza^e, Abdelmounim El Mrini^g, Denis Mercier^{a,b,c}, Elia d'Acremont^e, Marie-Odile Bristeau^e, Axel Creach^h

^a Laboratory of Physical Geography: Quaternary and Actual Environments (LGP-UMR 8591 CNRS), 4 rue Henri Dunant, 94320, Thiais, France

^b Sorbonne University, Geography and Planning Department, Paris, France, 1 rue Victor Cousin, 75005, Paris, France

^c Ocean Institute, Sorbonne University, 4 Place Jussieu, 75005, Paris, France

^d National Institute for Research in Digital Science and Technology (INRIA), 2 rue Simone Iff – CS 42112, 75589, Paris Cedex 12, France

^e Sorbonne University, CNRS-INSU, Paris Institute of Earth Sciences, ISTE², F-75005, Paris, 4 Place Jussieu, 75005, Paris, France

^f Probability, Statistics and Modelling Laboratory (LPSM - UMR 8001 CNRS), 4 Place Jussieu, 75005, Paris, France

^g LR3G, FS, Abdelmalek Essaadi University, M'hanache II District, 9 Avril Avenue, 2117, Tetouan, Morocco

^h CNRS, Université de Brest, Nantes Université, Université de Rennes, LETG, UMR 6554, F-29280, Plouzané, France

ARTICLE INFO

Keywords:

Exposure
Coastal hazard
Risk management
Alboran sea
Inundation maps

ABSTRACT

The Alboran Basin may be subject to tsunami hazards. If such an event were to occur, it is expected that the urbanised and densely populated areas of northern Moroccan coastline would be affected. Precise inundation hazard maps are needed for tsunami risk management in this region. In this article, we argue that the diversity of hazard mapping methods ensures the robustness of the scientific knowledge about the exposure of a territory. Hence, the main objective of this study is to analyse the exposure of the plain of Martil (north of Morocco), by using four hazard mapping methods to create inundation maps for two scenarios of tsunamis generated by extreme submarine mass failure (SMF) in the Alboran Sea, of 0.9 km³ and 3.8 km³ respectively. A digital terrain model of the plain was used to explore four methods of inundation mapping. The static method identified 4.32 km² and 19.83 km² of flooded areas for each scenario using water height values as inundation thresholds. The hybrid and the volumetric methods use the volume of water to determine the inundation extent. For the first scenario, 3.51 km² of the plain were inundated using the hybrid method, and 20.11 km² for the second scenario. The results of the volumetric methods are 2.32 km² and 7.82 km² respectively for the first and second scenario. Finally, the fourth method relies on numerical hydrodynamic modelling of tsunami inundation (Freshkiss3d® code). With this method, 4.55 km² of the plain were flooded in the first scenario, and 24.12 km² for the second. The comparison of the results highlights that the most sensitive areas to tsunami inundation are the lowest topographic ones, being the beaches and the wadis floodplains. This result raises questions on the current coastal development and the preparedness of its population, thus calling for more attention to engage on tsunami risk management related questions.

1. Introduction

The plain of Martil (north Morocco) is exposed to tsunami hazards taking source in the Alboran Sea (west Mediterranean), resulting from

either seismic events or submarine mass failure (SMF). Tsunamis are wave trains of long wavelength generated by a sudden displacement of the water column. They transport massive volume of water by radiating from their location of origin outward in all directions, with the power to

* Corresponding author. Laboratory of Physical Geography: Quaternary and Actual Environments (LGP-UMR 8591 CNRS), 4 rue Henri Dunant, 94320, Thiais, France.

E-mail addresses: elise.basquin@sorbonne-universite.fr (E. Basquin), apolline.el-baz@hotmail.fr (A. El Baz), jacques.sainte-marie@inria.fr (J. Sainte-Marie), alain.rabaute@sorbonne-universite.fr (A. Rabaute), maud.thomas@sorbonne-universite.fr (M. Thomas), sara.lafuerza@sorbonne-universite.fr (S. Lafuerza), a.elmrini@uae.ac.ma (A. El Mrini), denis.mercier@sorbonne-universite.fr (D. Mercier), elia.dacremont@sorbonne-universite.fr (E. d'Acremont), marie-odile.bristeau@inria.fr (M.-O. Bristeau), axel.creach@univ-brest.fr (A. Creach).

<https://doi.org/10.1016/j.nhres.2023.06.002>

Received 7 April 2023; Received in revised form 16 May 2023; Accepted 18 June 2023

Available online xxx

2666-5921/© 2023 National Institute of Natural Hazards, Ministry of Emergency Management of China. Publishing services provided by Elsevier B.V. on behalf of KeAi Communications Co. Ltd. This is an open access article under the CC BY-NC-ND license (<http://creativecommons.org/licenses/by-nc-nd/4.0/>).

penetrate inland when they reach shores (Papadopoulos, 2016). These forceful events could potentially affect the population of the plain and the local economy, as well as having indirect repercussions on the whole country (OECD, 2016).

Since 2000, around 32 tsunamis have caused about 252,000 deaths and 408.5 billion of dollars of damages around the world (National Geophysical Data Centre). Among these events, some fall under the scope of extreme events because of their magnitude (with a physical expression exceeding the norm usually observed) or their intensity (the power to cause damage and their extent) (Sharma, 2012). They are characterised by a low probability of occurrence. The 2004 Sumatra-Adaman (Indian Ocean) tsunami the 2011 Tōhoku (Japan) tsunami are considered as extreme both by magnitude and intensity. They resulted in the deaths of 230,000 and 18,500 people respectively, and generated about 10 and 220 billion of US\$ of damages. Inherently to their powerful nature, societies have few controls over tsunamis hazards. Nonetheless, they can act on the expected consequences of such hazards. Onshore impacts of these events have not been investigated for the north of Morocco. While the occurrence of such events is low (Papadopoulos and Fokaefs, 2013), it must be at heart of scientific investigation to prepare the populated Mediterranean coasts to their consequences, especially in the context of Morocco where tsunami risk management is still in development.

The international community shares methodologies to create inundation maps that they recommend to use as one of the cornerstone tools of tsunami risk mitigation and reduction (Løvholt et al., 2014; UNESCO/IOC, 2020). Nowadays, they are prerequisites for national guidelines reports (Ministry of Civil Defence and Emergency Management, 2016; Ministry of Land, Infrastructure, Transport and Tourism, 2012; US National Tsunami Hazard Mitigation Program, 2021). These maps evaluate the exposure of a given territory, which is understood as the spatial concomitance between the tsunami hazard and this territory. Thus, they are particularly useful for emergency and evacuation operations, but also to manage human occupation (Arreaga-Vargas et al., 2005; Tonini et al., 2021).

To our knowledge, such maps do not exist for the plain of Martil. However, it is one of the main populated areas within the Tanger-Tetouan-Al Hoceima region with a total population over 700,000 people spread over the prefecture of M'diq-Fnideq and the province of Tetouan (Haut Commissariat au Plan, 2014). As a seaside tourism spot, it is undergoing a coastal development process since the 1970's that is shaping the local socio-economic landscape (Aderghal, 2017, 2020), and is altering the natural environment with rapid urbanisation (Boulaassal et al., 2020; El Mrini et al., 2012b). This dynamic is reflected by the project of the Company of Development of the Valley of Wadi Martil (STAVOM) that plans to urbanise the floodplain of the main watercourse of the plain. It is supported by the government with the aim of creating or renovating urban areas and improving local services while increasing economic revenues (Paris Region Institute, 2020) (Fig. 1).

Considering this context, inundation maps would strongly condition the response to tsunami risk on the short and the long terms for the plain of Martil, and more widely for the northern coast of Morocco. This study analyses the exposure of the plain through the use of inundation maps created with four different methods (static, hydrodynamic, hybrid and volumetric), thus reflecting the geological surveys that have been undertaken by the interdisciplinary research program Evaluation of seabed hazards and risk analysis in the Mediterranean Sea (ALARM).

2. Scientific background

In tsunami science, different methods have been used to create inundation maps to study the exposure of Morocco to tsunami hazard. On the one hand, the inundation can be perceived through the analysis of sensibility factors that could condition the exposure to tsunami hazard. Taher et al. (2022) used a combination of terrain characteristics such as distance to the shore, altitude and slope as criteria to identify areas prone to tsunami inundation in the Nekor-Ghis bay, near the city of Al Hoceima.

On the other hand, numerical modelling has become the most common method to simulate tsunami inundation. In the case of Morocco, many numerical codes have been used and are presented in Table 1. The majority of these codes have been tested for seismic events set as input parameters and on the Atlantic coast of Morocco. Most of them use the Cornell Multi-grid Coupled Tsunami (COMCOT) and Simulating WAVes Nearshore (SWAN) codes that solve the shallow water equations with finite difference scheme. Seven studies out of nineteen studies focused on tsunamis effects in the Alboran Sea including two that use a submarine landslide type source event. Despite this prevalence, the Mediterranean studies show a more diverse panel of modelling codes. However, the associated work evaluated the impacts on the Spanish and Algerian coasts and provide few insights on the Moroccan one. Only Rodriguez et al. (2017) and Macías et al. (2015) elaborated simulations of SMF scenarios. Both studies explored the effects of submarine landslides that could occur in the south of the Alboran basin, at the southern flank of the Alboran Ridge and the northern flank of the Xauen-Tofino bank, respectively, thus observing the following tsunamis that could reach the Moroccan coast under 20 min with a 1m maximum water height at several locations of the coast.

Furthermore, extreme events scenarios have not been investigated for the north of Morocco. Only the famous 1755 event, supposed being the most destructive one in the Atlantic region, has been extensively studied (Amine et al., 2018a; Baptista et al., 2003; El Moussaoui et al., 2017; Omira et al., 2012; Ramalho et al., 2018; Tadibaght et al., 2022a). Overall, the 1755 Atlantic case prevalence and the lack of research on submarine landslide tsunamis are two reasons that justify the significant need to fill knowledge gaps on the exposure of the northern coast of Morocco to tsunamis. Using the case of the plain of Martil, these gaps will be addressed.

3. Study area

The plain of Martil is located on the northern coast of Morocco, facing the Spanish coast sitting on the Alboran Basin. It is constrained by the Rif mountains south and southwest (Fig. 1A-B) and by the cape of Cabo Negro (Fig. 1C-D) on the northeast. The city of Martil is constrained on a small hill (Fig. 2), between the Wadi El Maleh that has an irregular hydrologic regime, and the Wadi Martil which surrounds the district of Diza with a backwater (Fig. 1B, Fig. 2). An old channel is located south of the Wadi Martil (Fig. 2). The coastline is densely urbanised between Cabo Negro and the estuary of Martil Wadi and along the main road connecting Martil to Tetouan where the 2000 ha the Wadi Martil Valley project will be located. The shoreline is mainly composed of sandy beaches such as the Cabo Negro and Sidi Abdeslam (Fig. 1E-F, Fig. 2). In this study, the plain was delineated by identifying the areas below the break-of-slope set at a value of 2° of slope (Fig. 2). The total area of the plain is 57.73 km². It opens onto the Alboran Sea where tsunamis may be triggered by processes induced by the local geological context. This sea is a closed geological basin of relatively small size, delimited north by the Betic Cordillera, south by the Rif and Tell belts, west by the Strait of Gibraltar and east by the Algero-Balearic basin. In this westernmost part of the Mediterranean Sea, the current Eurasia-Nubia plates convergence and related African indentation are accommodated along two main strike-slip fault systems; the Al Idrissi and Yusuf fault systems (Estrada et al., 2018). Local seismicity considered as moderated (~6.4Mw) is mostly expressed in the Al-Idrissi strike-slip fault system (Gràcia et al., 2019; Grevemeyer et al., 2015). This Quaternary fault system is composed of a NNE-SSW oriented strike-slip sinistral structure that crosses the basin from Spain to the Moroccan coasts into the Al Hoceima bay (d'Acremont et al., 2014). Recent powerful events have affected this fault system in 1994 (6.0 Mw), in 2004 (6.4Mw) and in 2016 (6.3Mw) (Cherif et al., 2017). Within this fault system, some segments (e.g. Averroes Fault) exhibit vertical displacements and thus have been identified as the source of potential tsunamis generated by submarine earthquakes (Estrada et al., 2021). While several historical offshore earthquake episodes are

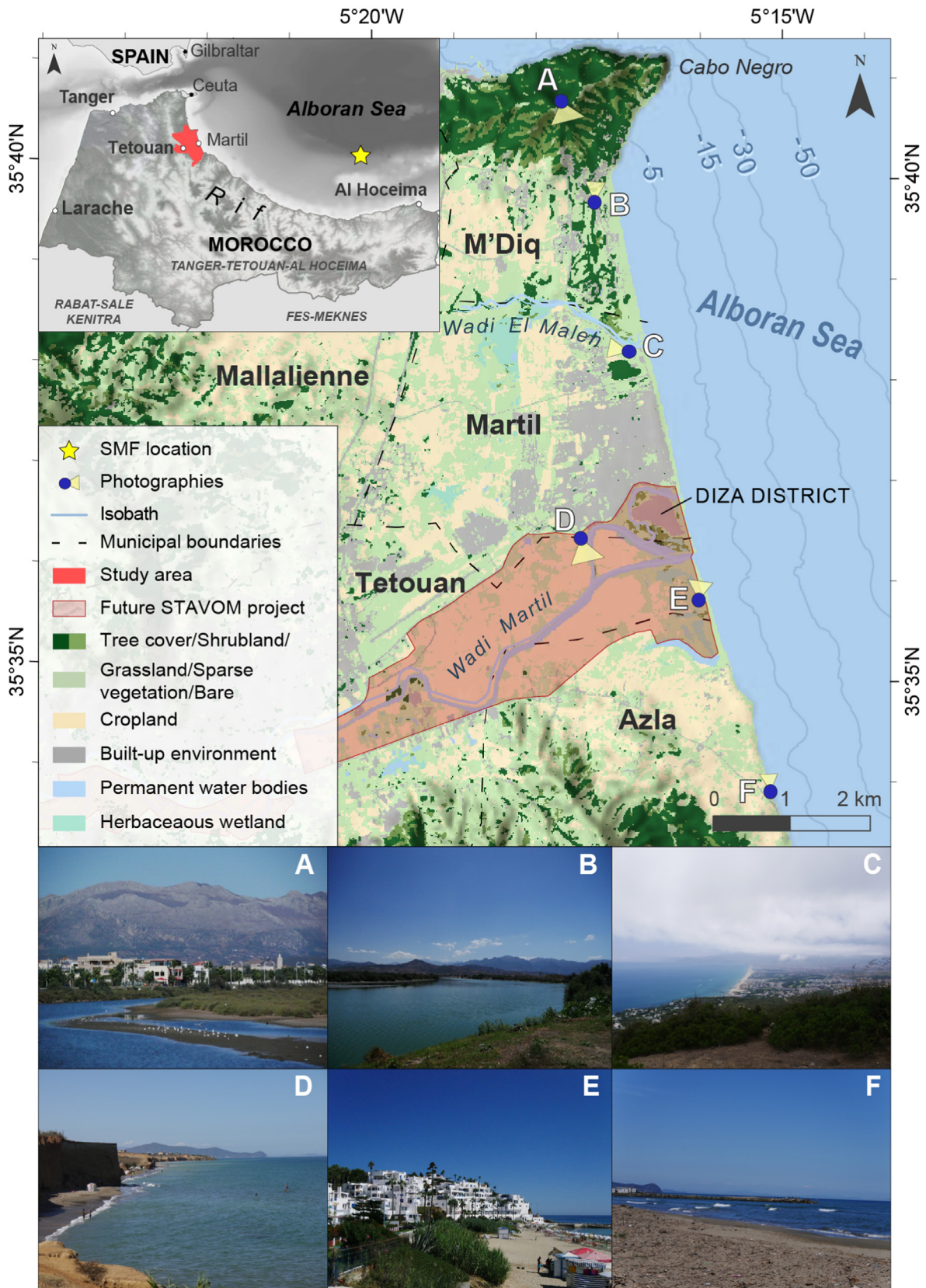


Fig. 1. Location of the plain of Martil. A. View from the downstream part of the Wadi El Maleh towards the back of the plain; B. View of the backwater of the Wadi Martil; C. The plain from the Cabo Negro military base; D. Cliffs located between the southern part of the Wadi Martil floodplain and the Azla urban zone, the Cabo Negro is seen in the background; E. Beach of Cabo Negro and its residential buildings; F. Beach of Sidi Abdeslam. (Source: MAXSAR, Microsoft, [GEBCO, 2021](#); USGS, 2014; Photographs taken in September 2021).

Table 1

Models used to study the exposure of Morocco and neighbour countries to tsunami hazards. Acronyms used in this table: SW = Shallow Water, B = Boussinesq, E = Euler, NS = Navier–Stokes, FD = Finite difference, FV = Finite volume, FE = Finite element, GP = Generation and Propagation, GPI = Generation, Propagation and Inundation.

| HYDRODYNAMIC MODELS | | | | | | | | |
|---|--|---------------------|---|--|-----------|--------------|----------------|--|
| Region studied | Source event | Model Name | Authors/Data | Spatial Dim. | Equations | Spatial Dis. | Phase modelled | |
| Alboran Sea | Submarine landslide (south Alboran ridge) | Shaltop + Freshkiss | This study | 3D | E/NS | FV/FE | GPI | |
| Alboran Sea | Submarine landslide (south Alboran ridge) | Tsunami-HySEA | Macías et al. (2015) | 2D | SW | FV | GPI | |
| Alboran Sea | Submarine landslides (Xauen-Tofino bank) | AVALANCHE | Rodríguez et al. (2017) | 2D | SW | FD | GP | |
| Alboran Sea (Spanish coast) | Seismic (five faults displacements) | RBREAK2 | González et Medina (1998) | 1D | SW | FD | GPI | |
| Alboran Sea (Algerian coast) | Seismic Scenario of the 1792 event | SWAN | Amir et Cisternas (2010) Amir (2014) | 2D | SW/NS | FD | GP | |
| Alboran Sea (Spanish coast) | Seismic (scenarios generated with PTHA method) | H2DTSU | González et al. (2010) (TRANSFER 2006–2009) | 2D | SW | FD | GP | |
| Alboran Sea (Spanish coast) | Seismic (1980, 2003) | COMCOT | Álvarez-Gómez et al. (2011) | 2D | SW | FD | GP | |
| Alboran Sea | Seismic (Averroes fault) | Tsunami-HySEA | Estrada et al. (2021) | 2D | SW | FV | GPI | |
| Atlantic coast | Seismic (1755 event) | SWAN | Baptista et al. (2003) | 2D | SW/NS | FD | GP | |
| Atlantic coast (Casablanca) | Seismic (1755 event) | COMCOT | Omira et al. (2010) | 1D/2D | SW | FD | GPI | |
| Atlantic coast (Rabat and Salé) | Seismic (1755 event) | TIDAL | Renou et al. (2011) | 2D | B | FD | GP | |
| Atlantic coast (Asilah) | Seismic (1755 event) | COMCOT-Lx | Mellas et al. (2012) Leone et al. (2012) | 2D | SW | FD | GPI | |
| Atlantic coast (S-E Iberian margin) | Seismic (1755 event) | COMCOT-Lx | Omira et al. (2012) | 1D/2D | SW | FD | GPI | |
| Atlantic coast (Cadiz Gulf) | Seismic | COMCOT-Lx | Omira et al. (2015) | 1D/2D | SW | FD | GPI | |
| Atlantic coast (Tangier) | Seismic (1755 event) | COMCOT-Lx | Benchekroun et al. (2015) | 1D/2D | SW | FD | GPI | |
| Atlantic coast (Asilah) | Seismic (1755 event) | COMCOT | El Moussaoui et al. (2017) | 2D | SW | FD | GPI | |
| Atlantic coast (Rabat) | Seismic (1755 and 1969 events) | SWAN | Amine et al. (2018a, 2018b) | 2D | SW/NS | FD | GP | |
| Atlantic coast (Tangier) | Seismic (1755 event) | COMCOT | Ramalho et al. (2018) | 2D | SW | FD | GPI | |
| Atlantic coast (Agadir) | Seismic (1755 event) | COMCOT | Fajri et al. (2021) | 2D | SW | FD | GPI | |
| Atlantic coast (El-Jadida to Tangier) | Seismic (1755 event) | TINTOL (NSWING) | Tadibaght et al. (2022a, 2022b) | 2D | SW | FD | GPI | |
| SUSCEPTIBILITY MAPS CREATED WITH GIS | | | | | | | | |
| Region studied | Source event | Model name | Authors | Factors included | | | | |
| Atlantic coast | Seismic | / | (Theilen-Willige et al., 2014) | Height levels (<10m), Terrain curvature (value = 0), Slope (<10°), Drop raster (<1000.000), High flow accumulation | | | | |
| Mediterranean coast, Nekor Bay (Al Hoceima) | Not mentioned | DAS model | (Taher et al., 2022) | Scoring of distance from shore, altitude and slope and multiplication of the scores | | | | |

proposed to have reached $\sim 7,1Mw$ (Álvarez-Gómez et al., 2011a, 2011b in Rodríguez et al., 2017), the strike-slip characteristic of the fault system yet limits the possibility of high tsunami elevations.

This regional proneness to seismic shaking is considered to be a trigger mechanism for seabed displacements and related SMF defined as downslope mass movement that transport sediments across the shallow continental slope to deeper parts of the ocean (Geertsema and Highland, 2011; Hampton et al., 1996). However, other characteristics of the Alboran Sea may play a role in tsunami generation. The complex basin seafloor presents morpho-structural features with a wide range of slope degrees (ridges, scarps, depressions). Geophysical data acquired in the southern part of the Alboran Sea during a series of oceanographic campaigns have allowed for the characterisation of the spatial distribution, of the volume and of the ages of submarine landslides (d'Acremont et al., 2022). Since the Quaternary, 66 submarine landslide processes have thus been identified with the SMF deposits volumes estimated between 0.01 and 15 km³. The main controlling mechanisms at the origin of the submarine landslides are the seismic shaking, the blind thrusts activity and the relatively high sedimentation rate of contourite deposits resulting from the circulation of water masses at the Gibraltar Strait. Contourite deposits could constitute weak sediment layers more sensitive to disruptions (Juan et al., 2016). In addition, the high sedimentation rate observed in the region corroborates with fluid escapes processes such as pore pressure phenomena which condition the initial stability of slopes

(d'Acremont et al., 2022; Alonso et al., 2021).

4. Materials and data

4.1. Scenarios of submarine landslides

The Alboran basin presents features that could explain its proneness to tsunami hazards triggered by SMF, some of them potentially being extreme events. Harbitz et al. (2014) claimed that the nature of SMF itself is extreme because of the wide variety of locations where they could occur (on passive or active continental margins) and on the wide range of values that their dimensions (mass discharge) and kinetic properties (acceleration, maximum velocity, mass discharge, and travel distance, etc.) can take. The underlying problem is that these parameters influence the tsunami magnitude, its travel time and its speed. Besides, observations and monitoring are difficult tasks to conduct on such hazards, making it almost impossible to predict them and demanding societies to prepare for these hazards blindly. This situation explains why historical earthquake records complemented with the geophysical data collected during a series of oceanographic campaigns (e.g. d'Acremont et al., 2022) are the main sources of information used to choose the scenarios for extreme tsunami simulations in this study. An event is mathematically considered as extreme whenever its severity has exceeded a certain fixed threshold. In this work, the severity corresponds to the total volume of

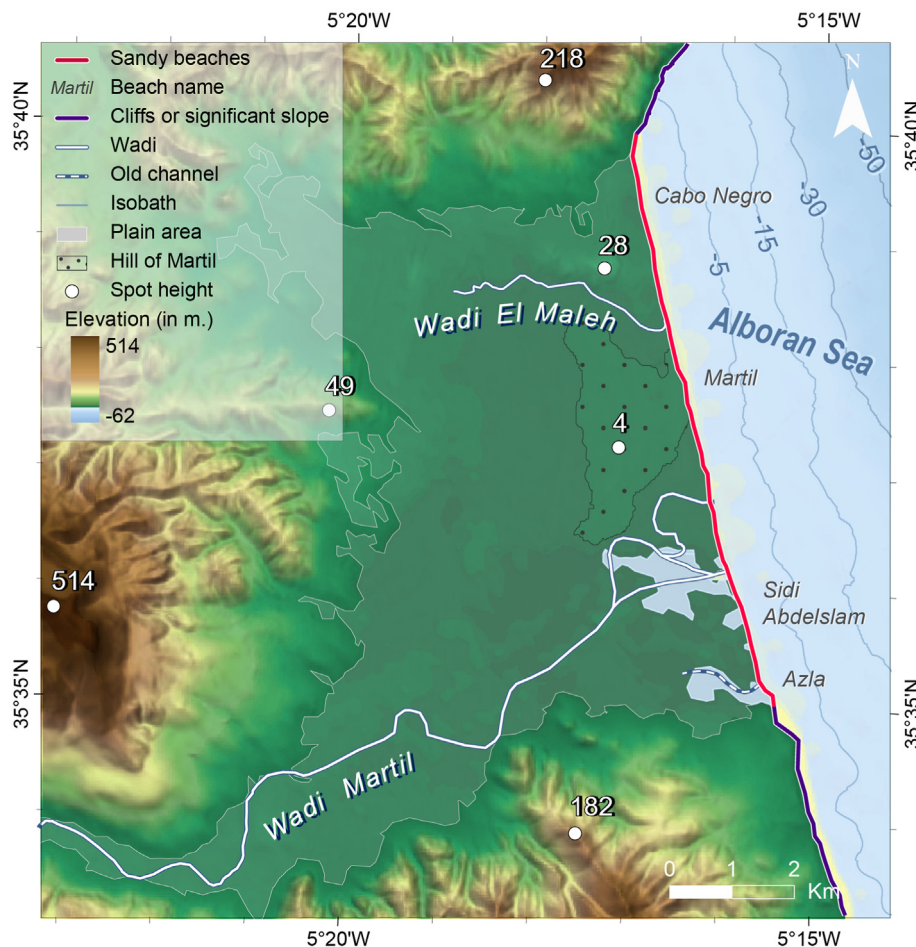


Fig. 2. Geomorphological map of the plain of Martil. The plain area was delineated by identifying all the areas under 2° of slope. (System of projection: WGS 1984 UTM Zone 30N; Source: USGS, 2014).

sediment displaced. This threshold was set at 0.15 km³, this value being the 0.47-quantile of the statistical distribution of the 66 quaternary submarine landslides deposits analysed in the Alboran Sea. The statistics are taken from the database built within the framework of the ALARM program from interpreted geophysical data collected during a series of oceanographic campaigns that contributed to the characterisation of extreme submarine landslides (Lafuerza et al., submitted). From these data, two scenarios of extreme events were chosen to consider different intensity levels of extreme events. The low intensity scenario is a scenario of a SMF of 0.9 km³ of displaced sediment with an estimated probability of occurrence estimated of 0.29 while the high intensity one is a 3.8 km³ SMF with an estimated probability of occurrence of 0.08. The choice for the latter scenario was motivated by the value of displaced sediment volume estimated for the great submarine landslide of Papua New Guinea that was followed by a tsunami in 1998 (Tappin et al., 2008).

Work prior from this study was numerically undertaken to model the generation and propagation phases of the two scenarios chosen. The generation of the two slides were simulated using the numerical code ShalTOP® to describe the continuous granular run-out of the sediments of each landslide over a reconstructed 2D swath-bathymetric data. This is a depth-averaged model based on the Saint-Venant hydrostatic equations and the Coulomb-type basal friction considering a Bingham rheology (Allgeyer et al., 2019; Bouchut and Westdickenberg, 2004; Lafuerza et al., submitted; Mangeney et al., 2007; Peruzzetto, 2021; Rabaute et al., 2022). The friction coefficient was set at 100 MPa to ensure the concordance between the slide scars and the deposit extent in the simulations. Then, these slide simulations were defined as the source parameters for the following propagation phase model, which required the

coupling between the ShalTOP code and the FREe Surface Hydrodynamics using KINetic SchemeS (Freshkiss3D) code, which are both on open access. The latter solves the 3D hydrostatic and incompressible Navier-Stokes equations in context of free surface and variable density flows. The two simulated slides were located at the same site on the northern flank of the Xauen-Tofino bank (Fig. 1) where the other landslides were identified (d'Acremont et al., 2022; Rodriguez et al., 2017).

Simulations results presented in Bristeau et al. (2022) show that the lowest scenario of a 0.9 km³ landslide would generate a wave in 8 min in the Alboran Sea domain, reaching the Moroccan coast in about 16 min near Al Hoceima. The tsunami arrives at the plain of Martil-Tetouan about 22 min after the beginning of the slide with a wave elevation of 0.4 m at sea and 0.6 m near the coast. For the second scenario, the tsunami arrives in 14 min to the shores of Morocco and 26 min at the studied plain. The wave elevation is about 1.4 m at sea, and 2 m near the coast of Martil. Both scenarios show how little time coastal societies have to react to such events. Thus, it is of utmost importance to investigate how these tsunamis would flood the plain of Martil.

Overall, choosing these scenarios aims to consider and understand the potential consequences that could result from hazards exceeding the norm, rare but possible. Their location implies that future events in this region could be threatening for the Moroccan coast due to short arrival time and high run-ups values. For further insights on the Alboran submarine landslides and their mechanisms, the reader can refer himself to Macías et al. (2015), Rodriguez et al. (2017) and more specifically d'Acremont et al. (2022) and Lafuerza et al. (submitted) which reflects the submarine landslide database used.

4.2. Topographic and bathymetric data

Determining accurate tsunami inundation requires precise topographic and bathymetric data to reflect accurately the inundation process. To build a consistent topography-bathymetry with a resolution high enough to be used in the modelling approach, we started from a Shuttle Radar Topography Mission Data (SRTM, Earth Resources Observation And Science Center (EROS), 2017) digital surface model (DSM) of the study area at 1 arc-sec resolution (~30 m) for the topography. The raster was smoothed to remove artefacts and errors (sinks for instance). Using an accurate land register for the city of Martil, indicating the locations of the buildings and housings, the pixels corresponding to the buildings in the DSM were removed to obtain a digital terrain model (DTM). We then interpolated these empty areas with the other pixels of the DSM, with constraints from a 1:7500 scale topographic map of the city of Martil, retrieved from the Moroccan National Agency for Land Conservation, Registry and Cartography (ANCFCC). At sea, measured depth soundings of a 1:50,000 scale nautical chart of the region made by the Spanish Instituto Hidrográfico de la Marina (IHM), were digitized and interpolated to create a bathymetry raster of greater resolution than those available for the study area. Finally, the two raster DTM were merged with a particular care to decide of a common altimetric reference level and to remove artefacts at the 0m isoline, to ensure a coherent continuity of the terrain.

5. Methods

5.1. Static method

According to the Intergovernmental Oceanographic Commission of the United Nations Educational, Scientific and Cultural Organisation (UNESCO-IOC), the basic method for creating inundation maps is the “bath-tub method”. It consists in applying a water height value to the topographic data of an area, which will distinguish flooded areas and non-flooded ones using elevation data (Fig. 3A). Since it only identifies

the water height and the spatial extent of the inundation it is considered as a static method. As mentioned previously, the water height set as the threshold was retrieved from the propagation models results and then applied onto our surface elevation raster. The raster cells below the water height defined for each scenario, that is 0.6 m for the 0.9 km³ scenario and 2 m for the 3.8 km³ one, were extracted. These values are only relevant to use for this region. Other location on the coast of Morocco could be exposed to different inundation water height according to the location of submarine landslides and their intensity (i.e. volume). For the method to be conclusive, the flooded areas must be connected to the seafront to guaranty the water penetration into the land. Consequently, isolated areas must be removed from the inundation extent. Here the runup value is understood as the difference between the elevation of the maximum tsunami penetration line and the mean sea level.

5.2. Hydrodynamic method

The hydrodynamic simulations of the tsunami inundation were performed using the numerical code Freshkiss3d® developed with in the ANGE team at Inria (Allgeyer et al., 2019). It is an open-source numerical code that can be retrieved from <https://freshkiss3d.gitlabpages.inria.fr/freshkiss3d/index.html>. It approximates the 3D incompressible hydrostatic Euler and Navier-Stokes systems with free surfaces. It uses a finite volume and finite element numerical schemes on fixed unstructured meshes and has wet/dry interfaces treatment. When the approximations are solved, the simulations provide several characteristics of the inundation. The first one is the flow rate arriving perpendicularly at the coast. Then the spatial extent of the inundated areas, the water height on land, the flow rate and the velocity rate of the water can be determined. These results can be withdrawn for every cell of the digital terrain model at different times during the inundation (Fig. 3B). The Freshkiss3d® model has been validated by Allgeyer et al. (2019) through different analytical solutions. No roughness coefficient was to simulate the land occupation. Notice the dynamic equations governing the displacement of the landslide has been simulated with the Shaltop code (Peruzzetto, 2021).

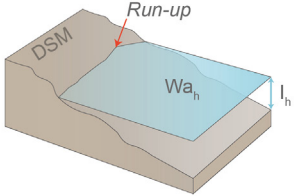
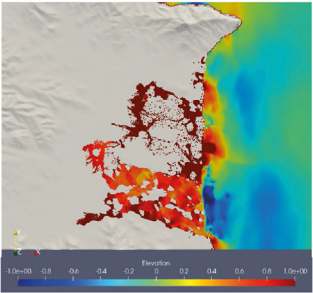
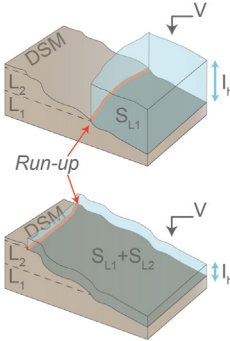
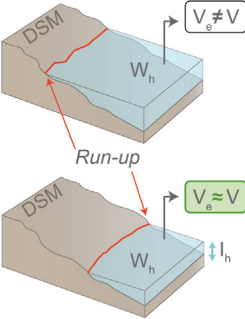
| A Static method | B Hydrodynamic method | C Hybrid method | D Volumetric method |
|--|---|--|--|
|  |  |  |  |
| $I_h = \text{DSM}_h - \text{Wa}_h$ <p>I_h = Inundation height (in m) DSM_h = Altitude/topography (in m) Wa_h = Tsunami wave height from the hydrodynamic propagation model (in m)</p> | <p>Freshkiss3D code</p> | $I_h = V_p / S_{L_x}$ <p>V = Inundation volume estimated by the numerical hydrodynamic model (in m³) S_{L_x} = Altimetric level surface (in m²) L_x = Altimetric level I_h = Inundation height (in m)</p> | $V_e = (S < W_h) \times W_h$ <p>If $V_e \approx V$ then $I_h = W_h - \text{DSM}_h$</p> <p>W_h = Water height tested (in m) S = Surface under W_h (in m²) V_e = Volume estimated under W_h (in m³) V = Inundation volume estimated by the numerical hydrodynamic model (in m³) I_h = Inundation height (in m) DSM_h = Altitude/topography (in m)</p> |

Fig. 3. Methods to determine tsunami inundation. The inundation height (I_h) is constant in the hybrid method only.

5.3. Hybrid method

The third method used is hybrid. It relies on the distribution of volumes of water by altimetric levels to obtain the water height at each of these levels considered (Fig. 3 C). The aim of using this method is to introduce the use of volume of water to create inundation maps since it is not commonly found in the literature.

The dynamic of the tsunami reaching the shores includes effects of reflection, refraction and diffraction of the waves (Sorensen, 2006; Bryant, 2014; Röbbke and Vött, 2017). Therefore, the volume considered to flood a territory is less significant than the volume propagating to a coast. In a consequence, the values of volume used in this method were retrieved from the results of the aforementioned numerical hydrodynamic inundation model. They were approximated using the average of water height and the geographical area. The volume of the lowest scenario of 0.9 km^3 is $316,296 \text{ m}^3$ of water. For the 3.8 km^3 scenario, it was estimated at $2,551,285 \text{ m}^3$ of water. The volumes were distributed until the water height reached at an altimetric level was less than 10 cm, meaning that the volume is not entirely depleted to avoid unrealistic spatial extents of inundations that exceed the plain's perimeter delineated as all areas under 2° of slope. The total volume could not be totally depleted or the spatial extent of the inundation would exceed the one of the plain. Hence, the tsunami runup is approximate and is deduced from the altimetric level reached at 0.10m water height.

In order to preserve the spatial continuity of the inundation, only adjacent cells of the raster have been followed in the distribution process. In this way, it was guaranteed that cells first appearing isolated from flooded areas, would be flooded only when the upper elevation level was filled with water.

5.4. Volumetric method

The fourth method to determine the inundation extent of the plain uses the same volumetric values previously mentioned in the hybrid method. However, its application process differs from the latter in that it considers the topographic elevation for the calculation of volumes and water height. The volume is estimated between the DTM and a water height and compared to the reference values (Fig. 3D). Different water heights are tested until the calculated volume corresponds approximately to the reference one. Once the correct water height is identified, the inundation height can be observed. The runup value is the water height level for which the volumes match.

6. Results

Two scenarios of submarine landslides generated tsunamis were explored, their inundations phases were modelled with the static method (S), the hydrodynamic (Hy), the hybrid (H) and the volumetric method (V). The scenario of a 0.9 km^3 landslide is defined as scenario 1, and the 3.8 km^3 slide is scenario 2.

The inundation extents are presented with similar water height thresholds to compare the exposure of the territory, and beyond, the level of danger the tsunamis would represent for the local population. They were set as less than 0.5m, between 0.5m and 1m, and more than 1m. They correspond respectively to the limit of mobility in still water for children or an elderly person, for a non-sporty adult and for a sporty adult under stress in a case of flooding (French Ministry of the Environment, Energy and the Sea, 2016). Parallels between human mobility limitations in flood and tsunami contexts have been made previously as they are both horizontal waves with the capacity to carry debris (Boschetti, 2020; Sahal, 2011).

Despite these common thresholds, caution must be taken into interpreting the resulting maps. While the static method, the hydrodynamic one and the volumetric method represent the water height (i.e. the difference between the topography and the level of water), the hybrid method shows the spatial extent at a specific water height set to be

studied. Thus, when considering a water height level, its extent includes the extent of previous higher levels. Also, for this method, the lowest water height level is set between 0.10m and 0.5m as the spatial extent. The water volumes are not totally distributed over the territory as this would lead to an overestimation of the inundation extent exceeding the plain's area.

6.1. Scenario of a 0.9 km^3 submarine landslide

In scenario 1, the static and the hybrid methods yielded similar results (Fig. 4-1S, 1H). Using the 0.6 m water height as the run-up value, the static method identified 4.32 km^2 of flooded surface up to 3.91 km inland, corresponding to 7.5% of the plain (Table 2). The inundation is concentrated near the Wadi Martil area and the old channel. In this area, the water height exceeds 0.5 m. Further inland, the flooding is located along the Wadi with a water height decreasing below 0.5 m which is the most prevailing level of water height. Overall, there is no area with a water height exceeding 1m. The maximum flooded zones delineated by the hybrid method for a water height set between 0.10 m and 0.5 m is about 3.51 km^2 and the equivalent run-up is between 0.4 and 0.5 m, about 3.48 km inland. This represents 6.1% of the plain, hence it is 18.9% less than the area identified by the static method. When the water height is set at 0.5 m, the inundation is mainly constrained around the Wadi Martil (Fig. 4-1H). When the volume of water is distributed further inland, the inundated areas follow the course of the Wadi as in the static method. The volumetric approach results show a similar, but smaller extent compared to the two first methods (Fig. 4 V). The volume of water concentrates in the wadi and channel respective bed. The inundation occupies 2.3 km^2 of the plain (4.1% of its territory), being 46.4% lesser than the static method and 34% than the hybrid one. For the first scenario, the volumetric method is the only one that does not identify inundation height higher than 0.5m. The runup is estimated at 0.38m of elevation around 2.95 km inland.

In terms of surface, the result from the hydrodynamic method is not substantially different. The total area inundated is about 4.55 km^2 (7.9% of the plain), only 5% larger than for the static method, but 22.9% more than the areas determined by the hybrid method and almost 50% than the volumetric method inundated areas. However, the inundation extent and height breakdown differ significantly from these two methods (Fig. 4-1Hy). While the Wadi Martil areas are flooded again with a more limited inland intrusion, the water is spreading all along the coast onto the beaches of Cabo Negro and Martil which is expected from this dynamic method that includes the effects of water coming from all direction offshore. Signs of intrusion are also visible in the outlet of the Wadi El Maleh The water height decreases as the water goes further inland, up to 2.83 km at a runup elevation of 0.39 m. Along the coast, it is greater than 0.5 m and 1m in specific locations. In the first 200 m inland from the shoreline, the height drops below 0.5 m as waters infiltrates further into the plain, except at the old channel of the Wadi where the inundation height is between 0.5 m and 1 m.

For this tsunami scenario, the four methods present some similar results of inundation (Fig. 5-1). They identify about 1.72 km^2 of common flooded surfaces in the Wadi Martil bed and the old channel which correspond to 25.6% of the total areas brought out (Table 3). All methods agree on the progression of water along the Wadi Martil. However, 45% of the inundation area is identified by only one method (3 km^2). It is partly explained by the result of the static method showing a slightly more intrusive inundation, but mostly because hydrodynamic method is the only one highlighting flooding of the majority of the coastline.

Essentially, in a case of an extreme event such as scenario 1 (0.9 km^3 SMF), the four approaches of inundation evaluation reveal that the plain is exposed to tsunami hazard along the shoreline. The results also pose the assumption that the Wadi Martil is a favourable factor for waters intrusion inland because of the low topography and weak slope of its floodplain.

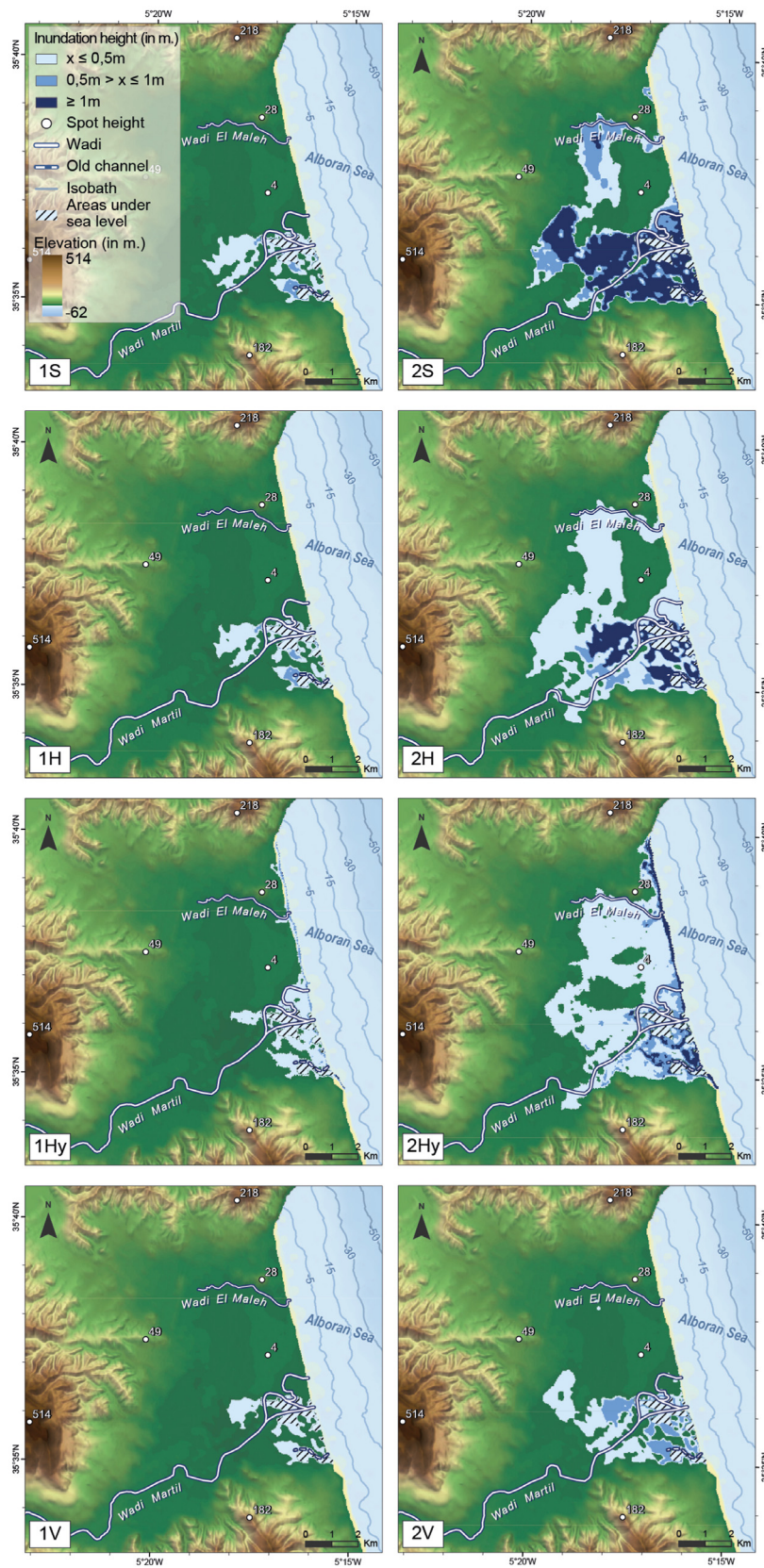


Fig. 4. Maps of the inundation results retrieved from testing two scenario of tsunamis (1 = 0.9 km³ of sediment displaced SMF, 2 = 3.8 km³ of sediment displaced SMF) with four methods of inundation evaluation (S = Static method; H = Hybrid method; Hy = Hydrodynamic method; V = Volumetric method). For the hybrid results maps, the lowest water height level must be interpreted as between 0.10 m and 0.5 m. (source: USGS, 2014; ANCFCC, 2011; IHM, 2021; OSM, 2020).

Table 2
Results of the four inundation determination methods and their degree of analogy.

| Scenario | Model type | Inundation method | | | | | Comparison of models | | |
|---------------------|--------------|---|---|------------------------------|--------------------|-----------------------------|-------------------------------|-------------------------------|-----------------------------------|
| | | Inundation surface area (in km ²) | Inundation surface area (in % of the plain) | Predominant inundation depth | Runup value (in m) | Tsunami penetration (in km) | Static (in km ² %) | Hybrid (in km ² %) | Volumetric (in km ² %) |
| 0.9 km ³ | Hydrodynamic | 4.55 | 7.9 | ≤ 0.5 m | 0.39 | 2.83 | -0.2 -5 | -1 -22.9 | 2.2 49.1 |
| | Static | 4.32 | 7.5 | ≤ 0.5 m | 0.6 | 3.91 | | -0.8 -18.9 | 2.01 46.4 |
| | Hybrid | 3.51 | 6.1 | 0.10 ≤ 0.5 m | 0.5 | 3.48 | | | 1.2 34 |
| | Volumetric | 2.32 | 4.1 | ≤ 0.5 m | 0.38 | 2.95 | | | |
| 3.8 km ³ | Hydrodynamic | 24.12 | 41.8 | ≥ 1 m | 2.37 | 6.35 | -4.3 -17.8 | -4 -16.6 | 16.3 67.6 |
| | Static | 19.83 | 34.4 | ≤ 0.5 m | 2 | 5.95 | | 0.3 1.4 | 12 60.6 |
| | Hybrid | 20.11 | 34.8 | 0.10 ≤ 0.5 m | 2.2 | 6 | | | 12.3 61.1 |
| | Volumetric | 7.82 | 13.6 | ≤ 0.5 m | 0.85 | 5.12 | | | |

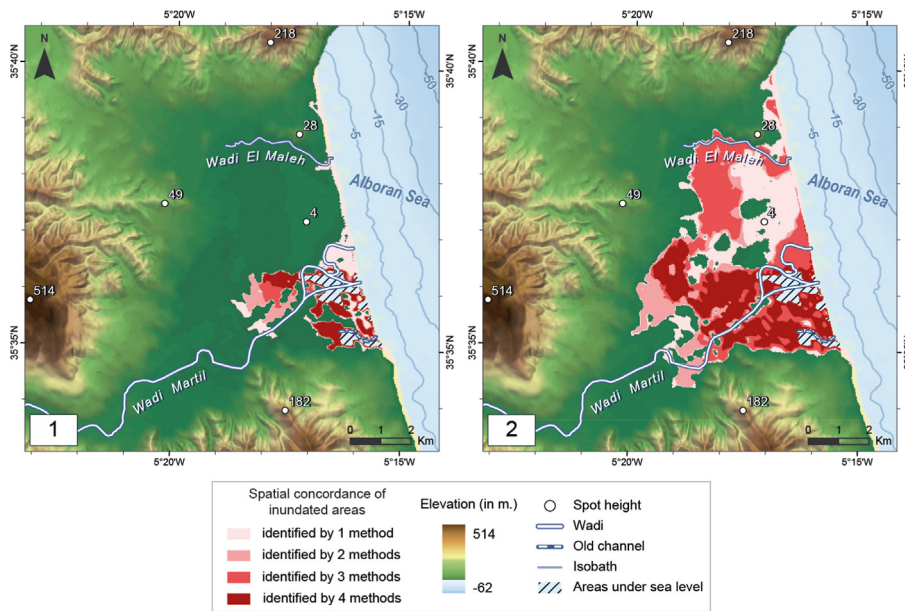


Fig. 5. Comparison of the spatial overlapping of the inundation extents identified by the four methods for each scenario of extreme tsunami events studied (1: scenario of a 0.9 km³ of sediment displaces submarine landslide; 2: scenario of a 3.8 km³ of sediment displaced submarine landslide) (source: USGS, 2014; ANCFCC, 2011; IHM, 2021; OSM, 2020).

6.2. Scenario of a 3.8 km³ submarine landslide

The results of the second scenario show how critically exposed the plain is to such extreme events. In the static approach, the water height or run-up value is 2 m which identifies 19.83 km² of flooded areas, representing 34.3% of the plain. At this 2m runup value, the waters reach 5.95 km inland. Contrary to the first scenario, the inundation does not only follow the Wadi Martil course up to the rear of the plain, but rather forms an arc behind the small hill of the city of Martil to reach the Wadi El Maleh (Fig. 4-2S). The southern part of the arc is characterised by significant water heights above 1m. Only the area around the district of Diza is mainly between 0.5 m and 1 m of water height. The northern part, next

to the Wadi El Maleh, is between 0.5m and 1m of water height but the area that connects the two parts falls below 0.5 m water height. Nonetheless, most of the inundation occurs in the floodplain or the Wadi Martil, including the old channel where the water height is over 1 m. Most of the external peripheral areas are under 0.5 m of water or less.

The hybrid approach reveals a slightly larger extent of 0.28 km² (1.4%) than the static method when the water height is set between 0.10m and 0.5m and reaches the altimetric level between 2.1 m and 2.2 m around 6 km inland (Fig. 4-2H). A total area of 20.11 km² is flooded, i.e. 34.8% of the plain. Its pattern is similar to the static method since it surrounds the small hill and connects the two Wadi through two channels. If the water height is set at 1m the flooding is constrained to the

Table 3

Level of spatial overlapping of the four inundation methods for the scenarios of extreme tsunami events studied.

| Level of overlap | Scenario 0.9 km ³ | | Scenario 3.8 km ³ | |
|------------------------------|-------------------------------|---|-------------------------------|---|
| | Surface (in km ²) | Share of the total inundation spatial extent (in %) | Surface (in km ²) | Share of the total inundation spatial extent (in %) |
| 1 method | 3.00 | 44.9 | 8.17 | 27.6 |
| 2 methods | 1.10 | 16.5 | 4.76 | 16.1 |
| 3 methods | 0.87 | 13 | 9.04 | 30.6 |
| 4 methods | 1.72 | 25.6 | 7.6 | 25.7 |
| Total areas inundated | 6.69 | 100 | 29.57 | 100 |

Wadi Martil. However, the lower the water height is, the more the inundation moves away from the back of the plain and starts to converge northwards, towards the Wadi El Maleh. For both static and hybrid methods of inundation determination, we can also note that a small area of the Cabo Negro beach is submerged below 0.5m of water or less.

Regarding the results of the hydrodynamic method, the inundation also highlights the significant potential of the inundation on the city of Martil and the outlets of both Wadi Martil and Wadi El Maleh (Fig. 4-2Hy). Nonetheless the surface flooded is 4 km² larger than for the first two methods. It represents 24.1 km² of the plain, thus comprising 41.8% of its surface. It is this 16.6% larger than for the hybrid method, and 21.6% more extended than the static one. The runup elevation is 2.37 m and the inundation distance is 6.35 km inland. The substantial differences with these methods are located in the northern half of the plain. First, the shoreline lying at the foot of the Cabo Negro is more extensively flooded under 1m and 0.5 m of water. Second, the hill of Martil is not spared in the hydrodynamic method. There, the inundation is less than or equal to 0.5m water height and flows to the rear of the plain then connects to the Wadi Martil floodplain through a narrower junction than for the first two methods. In the floodplain, the water height is mainly between 0.5 m and 1m but its lowest part towards the coast is below 1m of water or more, just like near the district of Diza. To the south, at the old channel, the water can also reach 1m of height, making the area between the latter and the Wadi the second most exposed zone in the plain after the coastline beaches, all of which are below under 1m of water or more.

The results of the volumetric method are significantly different (Fig. 4-2V). The territory onto which the volume is distributed is only 7.8 km², representing 13.6% of the plain. It is more than 60% lower than for each of the three other methods. The runup and the maximum inundation distance from the shoreline are also lower, being 0.85m of elevation and 5.12 km of distance respectively. However, results of the inundation spatial extent explain the path of water between scenario 1 and scenario 2 as they show how waters initiate their surrounding of the hill of Martil through a small basin at the bottom of the Rif mountains slopes with a water height under 0.5 m. It is the only method for which the inundation height does not exceed 1 m.

Overall, the spatial overlapping of the four methods under the condition of the second scenario is equal than for the first scenario (Fig. 5-2). 7.60 km² of inundated areas are commonly identified, representing 25.7% of the total flooded territory of 29.56 km² (Table 3). The static, the hybrid and the hydrodynamic methods highly coincide and constitute most of the 9.04 km² identified as flooded by three methods (30.6% of the inundation extent). Finally, the 8.17 km² area identified by one method mainly matches with the results of the hydrodynamic model. It corresponds to about one third of the total areas inundated. For this scenario, the methods confirm that the two wadis are vectors of water intrusion. Potentially, waters could be trapped behind the hill of Martil which is also exposed to flooding in the hydrodynamic model. More generally, it appears that the coastline and the Wadi Martil floodplain are the most exposed to extreme tsunami events.

7. Discussion

This study had two main objectives. On the one hand, this study aimed at assessing the exposure of the plain of Martil to investigate through hazard mapping how extreme tsunami events could affect the Mediterranean coast of Morocco. On the other hand, it focused on providing set of tools for tsunami inundation analysis for potential stakeholders interested risk management in an environment where high quality terrain data and tsunami run-up reference values are scarce.

7.1. Validation and limitations of the tsunami inundation determination methods

The latter of these objectives was addressed using four methods of tsunami inundation evaluation that were applied to an SRTM raster. Griffin et al. (2015) argued that using SRTM digital elevation data may lead to an underestimation of the inundation extent, as the elevation data tends to be overestimated. However, Tufekci-Enginar et al. (2022) showed that they present fewer errors in inundation modelling than other open-source digital elevation models. The SRTM raster used to study the plain of Martil was modified to limit such errors and it was combined with bathymetric data improving the precision for the hydrodynamic model. It has a 25m mesh resolution which Griffin et al. (2015) found to be suitable to analyse tsunami inundation, even though a higher resolution would provide a better understanding of flow progression, especially in rivers. Moreover, the Wadi Martil has been recently recalibrated to support the development of the STAVOM company project, which that will urbanise the Wadi floodplain (Paris Region Institute, 2020) and prevent such events from damaging the plain. Future projects also aim to create a new terminal for Tetouan airport, as well as a new take-off runway, which will modify the trajectory of the road connecting Tetouan to Martil (National Office of Airports, 2023). These works changed or will modify the local topography which implies that future work on the coastal environment of Morocco should be considered to obtain higher up-to-date resolution digital terrain model, preferably with elevation determination using LIDAR data.

One could also question the relevance of low probability, high impact events such as the selected scenarios (see 4.1). However, as it is a general conception in hazard studies, especially when they are studied under the scope of extreme value theory, that the absence of risk is non-existent. Thus, evaluating their magnitude and the extent of their effects on land is an important means of anticipating the potential associated dramatic consequences. To pursue the investigation about tsunami effects on the plain of Martil and more generally on the northern coast of Morocco, other scenarios must be explored. Indeed, the two scenarios studied result from similar mechanisms of SMF that were triggered at the same location in the slide and propagation simulations. This explains that the inundation intensity between the two scenarios is proportional to the magnitude of the SMF considered. Furthermore, multihazards scenario of extreme events deserve scientific attention (Raymond et al., 2020; Sadegh et al., 2018), especially in a region where tsunami could also be generated by the nearby Al Hoceima seismic activity (Álvarez-Gómez et al., 2011a). The concomitance of tsunami inundation and an event of flooding from the Wadi Martil could also be a possible scenario since they are regular phenomena. The most recent flooding episodes took place in 1998, 2000 and 2006 causing several deaths and millions of Dirhams of casualties (Karrouchi et al., 2016).

The four inundation methods used in this study were all able to provide exploitable results for understanding the effects of two of extreme tsunami scenarios. Table 4 summarises all the factors involved in the inundation phase of the tsunami that are included in the different methodology approaches, along with the results that can be expected for each method. The static method is advantageous because of its low-cost and time-efficient approach, but also because of the possibility of

Table 4

Summary of input parameters and outputs characteristics of the four inundation evaluation methods. Yes = For the static, hybrid and volumetric methods, the direction of flow is deduced from the comparison between the two scenarios and not through a reproduction of the kinetic aspect of the inundation.

| | | Static | Hybrid | Volumetric | Hydrodynamic |
|---|-------------------------------|--------------------|---|---|-------------------|
| Factors influencing the inundation | Slope variation | No | No | No | Yes |
| | Near-shore bathymetry | No | No | No | Yes |
| Results of methods | Land use | No | No | No | Can be included |
| | Spatial extent | Yes | Yes | Yes | Yes |
| | Inundation height | Yes | Yes (constant) | Yes | Yes |
| | Speed of flow | No | No | No | Yes |
| | Direction of flow | Yes | Yes | Yes | Yes |
| | Time span of the event | No | No | No | Yes |
| | Runup | Maximum elevation | Maximum elevation in the altimetric level reached | Maximum elevation in the altimetric level reached | Maximum elevation |
| Time and ease of execution | Short/easy | Long/requires care | Medium/easy | Long/Requires high computation equipment | |
| Spatial precision | Approximate | Approximate | Approximate | High | |

modulating the water height used as reference, which explains why it is praised by international institutions as the first method to use when none others can be developed (UNESCO/IOC, 2020). Yet, it only provides primary insights on how the inundation would happen, just as does the hybrid method, but the latter is time-demanding. To our knowledge, volumes of water displaced during a tsunami have not been exploited as references for tsunami inundation evaluation to our knowledge, except under numerical modelling techniques. Run-up values are more accessible, thus usually preferred to study the inundation phase. Still, as tsunamis are rare events, and SMF ones are difficult to monitor, it could be argued that using volumetric data to assess tsunami inundation could compensate the absence of reliable run-up data or the impossibility to develop numerical modelling. Hence, the volumetric method is useful for such analysis and present itself as a quick and easy way to assess tsunami inundation.

Static, hybrid and volumetric methods are both used to determine the spatial extent and the water height of the flooding can be determined. These are two of the main criteria used to analyse the magnitude of an inundation and to apprehend water motion vertically and horizontally. Nevertheless, it is clear that the hydrodynamic model is the most comprehensive out despite its high numerical cost, the specific computation equipment and expertise it requires (high memory computer, high-speed processor, etc.). It presents some clear advantages to use as it provides velocity data (i.e. speed and direction of flow), highlights the temporal dimension of the inundation and is the only method to apprehend how the near-shore bathymetry, the topographic variations and the energy dissipation act as the inundation progress further inland.

However, it is important to note that there may be uncertainties in terms of inundation extent. They are inherent to any inundation model (Sugawara, 2021). The infinite number of possible scenarios of this complex tsunami phenomenon and the errors margin of the modelling techniques may lead to a rough estimate of the inundation. In this study, the results obtained may lean towards the side of overestimation, especially in the cases of the hybrid and static methods, even though the volumetric method seems to underestimate the inundation compared to the latter. According to the recommendations of UNESCO/IOC (2020), uncertainties that tend to overestimate the results are assumed to be credible, but above all justified, as they lead towards the safety of populations and their assets. But they also come with the risk of unnecessary evacuation of areas in case of a tsunami which has social and economic costs. The results of the hydrodynamic model are therefore preferred to highlight the sensitivity of the physical environment of the plain to tsunami inundation in terms of heights and surface. However, in some extents, the static, the hybrid and the hydrodynamic methods can be used to validate and complement the results of the hydrodynamic model, especially because benchmark analytical laboratory and field tests are not possible in this context as it is recommended to validate a model

(Synolakis et al., 2008). In addition, Harbitz et al. (2006) state that hydrodynamic numerical modelling is the key to understanding and predicting submarine landslides and explains all the important developments that this discipline is undergoing (Behrens and Dias, 2015; Marras and Mandli, 2021; Sugawara, 2021).

7.2. Exposure of the plain of Martil to extreme tsunami events

The assessment of the exposure to extreme tsunami hazards was performed through the mapping of the inundation phase of two scenarios of extreme tsunamis for the plain of Martil. The results found in the plain of Martil suggest that the two Wadis are factors facilitating the progression of water inland up to 3.91 km in the Wadi Martil floodplain in the 0.9 km³ scenario and up to about 6.35 km in the 3.8 km³ scenario (Table 2, Fig. 5). For the latter scenario, water could penetrate about 3 km inland due to the morphology of the Wadi El Maleh. This corroborates studies that have observed tsunami behaviours in rivers mouths (Suppasri et al., 2017; Tsuji et al., 1991; Yamanaka and Shimozono, 2022) and in extreme events contexts such as the 2004 Indian Ocean tsunami (Borrero et al., 2006; Liew et al., 2010), the 2011 Tohoku tsunami (Chini et al., 2013; Goto et al., 2011) or the 1755 great tsunami of Lisbon (Renou et al., 2011; Tadibaght et al., 2022b).

Nonetheless, considering the aim of the article to assess the exposure of the plain and study the morphological forms that could enhance or limit the penetration of water, the land use and occupation have not been integrated in any of the methods while the use of a roughness factor to study these elements effects is often seen in the literature (Fukui et al., 2019; Gayer et al., 2010; Kaiser et al., 2011; Sadeh et al., 2018). Therefore, the resulting extents of inundation can be discussed, especially in the first scenario where the inundation seems constrained to the coast and the downstream area of Wadi Martil. One could assume that the near-coast bathymetry and beaches morphologies act as natural barriers and attenuate the inundation. In fact, subtidal bars are bars observed in the first 500 m of the subtidal zone (El Mrini, 2011). Even though the bathymetry is mostly parallel to the coastline, such elements could disrupt the tsunami gain of energy at such near-shore distance, but these effects are challenging to evaluate (Lynett, 2016). Beach morphology could also influence the overpassing of the tsunami onto the land. According to El Mrini (2011) there is a difference of 3 m of altitude over a distance cross-shore of 135 m at Sidi Abdeslam beach (Fig. 1F). For the beach of Martil, the gap is about 4 m over a distance of 90 m. It decreases to 2.5 m over 120 m at Cabo Negro beach. However, chronic coastal erosion, characterised by dune environment degradation, due to urbanisation processes, have deleterious effects during storm flooding episodes (El Mrini et al., 2012a, 2012b). The destruction of such environments could also prevent natural mitigation effects when tsunami submersion.

Overall, the results of the inundation assessment methods allowed us

to examine the level of danger that the inundation would represent for the local population. For the first scenario, children, elderly and non-sportive adults would be in danger if located in the Wadi Martil floodplain where waters easily reach 0.5m of height. Also, sportive adults under stress would be exposed to danger in beaches as the water height reaches 1m in these areas. For the second scenarios these conclusions are exacerbated as all beaches are below 1m of water height and the downstream areas of Wadi Martil are also 0.5m of water height. Nonetheless, these levels of danger are estimated without the kinetic aspect of an inundation (0 m/s) and tsunami are non-static phenomenon that have the capacity to carry debris. Consequently, the level of threat presented here should be taken with caution as they probably underestimate the danger.

Finally, overlapping inundations extents between the four methods are analysed as the most susceptible to tsunami inundation (Fig. 5). The 0.9 km³ SMF scenario showed that the majority of the flooding would be located near the floodplain of the Wadi Martil and the many beaches of the coast, which correlates with their low topographic elevation and their connection to the sea. These observations are verified in the scenario of the 3.8 km³ SMF tsunami in which they are more exposed in terms of surface and water height. Additionally, in this scenario, waters surround the hill of Martil city, isolated from the rest of the plain. Most of these parts of the plain are highly urbanised. The seafront of Martil city and the beaches north of Wadi Martil are equipped to welcome tourists during the high season. Many housing projects are under construction in the rest of the plain and local amenities are developed to answer the needs of the permanent population, usually working in Tetouan, as well as the seasonal one. Besides, the floodplain of Wadi Martil is the heart of the future STAVOM coastal development project (Paris Region Institute, 2020) which will densify drastically the plain and thus aggravate its exposure. Considering the configuration of the plain and its development perspectives, the hazard maps elaborated in this study find their utmost interest as tsunami risk management tools. They condition short- and long-term responses to such hazard, which explains why they are used for diverse risk management applications such as for evacuation strategies, conveyance of emergency supply, adaptation of urban planning, vulnerability assessments, etc.

8. Conclusion

As the first step to help mitigate tsunami risk (Baba et al., 2014), hazard mapping must be undertaken with precaution and must be discussed. In this study, four methods of inundation evaluation have been used to create these exposure assessment maps of the plain of Martil (north Morocco). The combination of the four methods proved to be useful in bringing scientific knowledge about SMF tsunamis in the Moroccan coastal environment where the effects of this type of tsunamis have not been thoroughly researched previously. Two scenarios of extreme SMF generated tsunamis, based from geological study were investigated to assess and envision different degrees of exposure according to the magnitude of these hazards. The comparison of their respective results allowed the identification of the inundation prone areas of the plain of Martil. The first scenario of a 0.9 km³ SMF revealed that the seafront and beaches would be highly exposed as well as the lowest part of the Wadi Martil floodplain. The second scenario of a 3.8 km³, showed that when the tsunami is more intense, the inundation progresses towards the back of the plain surrounding the city of Martil, mainly due to the intrusion of water through the two Wadis. The general plain environment of the plain facilitates this propagation but local subtidal bars and the beaches morphology could be factors of inundation attenuation. The case of the plain of Martil confirms the long-time observation that hydrodynamic modelling is the most complete method to appreciate the flooding, and we advocate for its use, especially to study inundation in local context such as this one. The static method, while approximate, is the most easily and fast method to use and we recommend to use it, especially in case of tsunamis with short arrival time when

hydrodynamic modelling is not feasible. Using the volumetric and hybrid methods can constitute useful processes to apprehend tsunami inundation, though they require more care to be processed and reference volumetric data of tsunami inundation are not common in the literature.

For local authorities, and more generally for risk management stakeholders, these maps provide a first approach of tsunami inundation which can help establishing guidelines to prepare the Mediterranean coast of Morocco to future potential events and to mitigate the effects of extreme events. As no prevention and strategic plans exist to this day for this type of hazard (World Bank, 2014; OECD, 2016), this study is a first step taken that could lead to reflexions on the directions taken for urban planning and coastal development in this region. The maps elaborated can also be used as a support to for evacuation maps, emergency planning and to raise the awareness of the population on such risk as hazard mapping remains one of the key domains of tsunami mitigation and preparedness (Dengler, 2005; González et al., 2005; Bernard et al., 2006; Dransch et al., 2010). Therefore, these inundation maps could highly condition the response to tsunami risk on the short and the long terms for the plain of Martil, and more widely for the northern coast of Morocco.

Declaration of competing interest

The authors declare that they have no known competing financial interests or personal relationships that could have appeared to influence the work reported in this paper.

Acknowledgments

This work is part of the Evaluation of seabed hazards and analysis of risks in the Mediterranean Sea (ALARM) funded by the program EMERGENCE of Sorbonne University and the mission for transversal and interdisciplinary initiatives (MITI) of CNRS and IRD institutes. We thank the Ocean Institute from Sorbonne University for funding the scholarship of the PhD Elise Basquin. We are grateful for the help of professor Driss Nachite from Abdelmalek Essaâdi University (Morocco) who provided the nautical chart that allowed us to have precise bathymetric data. We are also thankful to Bruno Scalabrino (Côte d'Azur University, France) who provided the DSM data that increased the quality of the analysis. The authors acknowledge Anne Mangeney (IPGP, France) and Marc Perruzeto (BRGM, France) for fruitful discussions concerning the capabilities of the Shaltop code for simulation of landslides.

References

- Aderghal, S., 2017. Pratiques touristiques et espace de séjour. Cas des estivants marocains sur le littoral de Tétouan. *GéoDév.ma* 5. <https://doi.org/10.48343/IMIST.PRSM/geodev-v5.11352>.
- Aderghal, S., 2020. Tourisme et dynamiques territoriales sur le littoral de Tétouan. *GéoDév.ma* 8. <https://doi.org/10.48343/IMIST.PRSM/geodev-v8.22727>.
- Allgeyer, S., Bristeau, M.-O., Froger, D., Hamouda, R., Jauzein, V., Mangeney, A., Sainte-Marie, J., Souillé, F., Vallée, M., 2019. Numerical approximation of the 3D hydrostatic Navier–Stokes system with free surface. *ESAIM: M2AN*. 53 (6), 1981–2024. <https://doi.org/10.1051/m2an/2019044>.
- Alonso, B., Juan, C., Ercilla, G., Cacho, I., López-González, N., Rodríguez-Tovar, F.J., Dorador, J., Francés, G., Casas, D., Vadorpe, T., Vázquez, J.T., 2021. Paleooceanographic and paleoclimatic variability in the Western Mediterranean during the last 25 cal. kyr BP. New insights from contourite drifts. *Mar. Geol.* 437, 106488. <https://doi.org/10.1016/j.margeo.2021.106488>.
- Álvarez-Gómez, J.A., Aniel-Quiroga, I., González, M., Otero, L., 2011a. Tsunami hazard at the Western Mediterranean Spanish coast from seismic sources. *Nat. Hazards Earth Syst. Sci.* 11 (1), 227–240. <https://doi.org/10.5194/nhess-11-227-2011>.
- Álvarez-Gómez, J.A., Aniel-Quiroga, I., González, M., Olabarrieta, M., Carreño, E., 2011b. Scenarios for earthquake-generated tsunamis on a complex tectonic area of diffuse deformation and low velocity: the Alboran Sea, Western Mediterranean. *Mar. Geol.* 284 (1), 55–73. <https://doi.org/10.1016/j.margeo.2011.03.008>.
- Amine, M., Oudaf, L., Baba, K., Bahi, L., 2018a. Assessment of the tsunami hazard on Moroccan coasts using numerical modeling. *MATEC Web Conf* 149, 02079. <https://doi.org/10.1051/mateconf/201814902079>.
- Amine, M., Latifa, O., Bahi, L., Baba, K., Astier, S., 2018b. Establishment of a process of tsunami risk mapping modeling in a 3D video for the city of Rabat-Morocco: application to the worst scenario 1755 and the moderate scenario 1969. *Int. J. Civ. Eng. Technol.* 9 (9), 1559–1572.

- Amir, L., 2014. Tsunami hazard assessment in the Alboran Sea for the western coast of Algeria. *J. Shipp. Ocean Eng.* 4, 43–51.
- Amir, L., Cisternas, A., 2010. Appraisal of the 1790 Alboran Tsunami Source in the West Mediterranean Sea as Inferred from Numerical Modelling: Insights for the Tsunami Hazard in Algeria. U.S. National and 10th Canadian Conference on Earthquake Engineering, Vancouver, Canada, p. 9. Presented at the 9th.
- Arreaga-Vargas, P., Ortiz, M., Farreras, S.F., 2005. Mapping the possible tsunami hazard as the first step towards a tsunami resistant community in esmeraldas, Ecuador. In: Satake, K. (Ed.), *Tsunamis: Case Studies and Recent Developments, Advances in Natural and Technological Hazards Research*. Springer Netherlands, Dordrecht, pp. 203–215. https://doi.org/10.1007/1-4020-3331-1_12.
- Baba, T., Takahashi, N., Kaneda, Y., Inazawa, Y., Kikkojin, M., 2014. Tsunami inundation modeling of the 2011 Tohoku earthquake using three-dimensional building data for Sendai, Miyagi prefecture, Japan. In: Kontar, Y.A., Santiago-Fandiño, V., Takahashi, T. (Eds.), *Tsunami Events and Lessons Learned: Environmental and Societal Significance, Advances in Natural and Technological Hazards Research*. Springer Netherlands, Dordrecht, pp. 89–98. https://doi.org/10.1007/978-94-007-7269-4_3.
- Baptista, M.A., Miranda, J.M., Chierici, F., Zitellini, N., 2003. New study of the 1755 earthquake source based on multi-channel seismic survey data and tsunami modeling. *Nat. Hazards Earth Syst. Sci.* 3 (5), 333–340. <https://doi.org/10.5194/nhess-3-333-2003>.
- Behrens, J., Dias, F., 2015. New computational methods in tsunami science. *Phil. Trans. R. Soc. A.* 373 (2053), 20140382. <https://doi.org/10.1098/rsta.2014.0382>.
- Benchekroun, S., Omira, R., Baptista, M.A., Mouraouah, A.E., Brahim, A.I., Toto, E.A., 2015. Tsunami impact and vulnerability in the harbour area of Tangier, Morocco. *Geomatics, Nat. Hazards Risk* 6 (8), 718–740. <https://doi.org/10.1080/19475705.2013.858373>.
- Bernard, E. n, Mofjeld, H. o, Titov, V., Synolakis, C. e, González, F. i, 2006. Tsunami: scientific frontiers, mitigation, forecasting and policy implications. *Phil. Trans. R. Soc. A.* 364, 1989–2007. <https://doi.org/10.1098/rsta.2006.1809>.
- Borrero, J.C., Sieh, K., Chlieh, M., Synolakis, C.E., 2006. Tsunami inundation modeling for western Sumatra. *Proc. Natl. Acad. Sci. USA* 103 (52), 19673–19677. <https://doi.org/10.1073/pnas.0604069103>.
- Boschetti, L., 2020. *Le risque de tsunami dans les Alpes-Maritimes, quelles réalités ? Quelles méthodes d'analyses de l'aléa et de la vulnérabilité ?* (PhD thesis) Université Côte d'Azur.
- Bouchut, F., Westdickenberg, M., 2004. Gravity driven shallow water models for arbitrary topography. *Commun. Math. Sci.* 2 (3), 359–389. <https://doi.org/10.4310/CMS.2004.v2.n3.a2>.
- Boulaassal, H., Anaki, S., Yazidi, O.A., Maatouk, M., Wahbi, M., 2020. Cartographie des changements de l'occupation du sol entre 2002 et 2016 à partir des images Landsat. Cas de la région Tanger Tetouan Al-Hoceima (Maroc). *Afr. J. Land Pol. Geospatial Sci.* 3 (2), 14–31. <https://doi.org/10.48346/IMIST.PRSM/ajlp-gs.v3i2.19288>.
- Bristeau, M.-O., Baz, A.E., Sainte-Marie, J., Team, A., Lions, L., 2022. *Submarine Landslides and Tsunami in the Alboran Sea*. Working Paper. 23.
- Bryant, E., 2014. Tsunami dynamics. In: Bryant, E. (Ed.), *Tsunami: the Underrated Hazard*. Springer International Publishing, Cham, pp. 19–32. https://doi.org/10.1007/978-3-319-06133-7_2.
- Cherif, S., Chourak, M., Abed, M., Pujades, L., 2017. Seismic risk in the city of Al Hoceima (north of Morocco) using the vulnerability index method, applied in Risk-UE project. *Nat. Hazards* 85 (1), 329–347. <https://doi.org/10.1007/s11069-016-2566-8>.
- Chini, M., Piscini, A., Cinti, F.R., Amici, S., Nappi, R., DeMartini, P.M., 2013. The 2011 Tohoku (Japan) tsunami inundation and liquefaction investigated through optical, thermal, and SAR data. *IEEE Geosci. Rem. Sens. Lett.* 10 (2), 347–351. <https://doi.org/10.1109/LGRS.2012.2205661>.
- Dengler, L., 2005. The role of education in the national tsunami hazard mitigation program. In: Bernard, E.N. (Ed.), *Developing Tsunami-Resilient Communities: the National Tsunami Hazard Mitigation Program*. Springer Netherlands, Dordrecht, pp. 141–153. https://doi.org/10.1007/1-4020-3607-8_9.
- Dransch, D., Rotzoll, H., Poser, K., 2010. The contribution of maps to the challenges of risk communication to the public. *Int. J. Digit. Earth.* 3 (3), 292–311. <https://doi.org/10.1080/17538941003774668>.
- d'Acremont, E., Gutscher, M.-A., Rabaute, A., Mercier de Lépinay, B., Lafosse, M., Poort, J., Ammar, A., Tahayt, A., Le Roy, P., Smit, J., Do Couto, D., Cancouët, R., Prunier, C., Ercilla, G., Gorini, C., 2014. High-resolution imagery of active faulting offshore Al Hoceima, Northern Morocco. *Tectonophysics* 632, 160–166. <https://doi.org/10.1016/j.tecto.2014.06.008>.
- d'Acremont, E., Lafuerza, S., Rabaute, A., Lafosse, M., Jollivet Castelot, M., Gorini, C., Alonso, B., Ercilla, G., Vazquez, J.-T., Vandorpe, T., Juan, C., Migeon, S., Ceramicola, S., Lopez-Gonzalez, N., Rodriguez, M., El Moumni, B., Benmarha, O., Ammar, A., 2022. Distribution and origin of submarine landslides in the active margin of the southern Alboran Sea (Western Mediterranean Sea). *Mar. Geol.* 445, 106739. <https://doi.org/10.1016/j.margeo.2022.106739>.
- Earth Resources Observation And Science (EOS) Center, 2017. Shuttle Radar Topography Mission (SRTM) 1 Arc-Second Global. <https://doi.org/10.5066/F7PR7TFT>.
- El Moussaoui, S., Omira, R., Zaghoul, M.N., El Talibi, H., Aboumaria, K., 2017. Tsunami hazard and buildings vulnerability along the Northern Atlantic coast of Morocco –the 1755-like tsunami in Asilah test-site. *Geoenviron. Disasters* 4 (1), 25. <https://doi.org/10.1186/s40677-017-0089-6>.
- El Mrini, A., 2011. *Evolution morphodynamique et impact des aménagements sur le littoral tétouanais entre Ras Mazari et Fnideq (Maroc Nord Occidental)* (These de doctorat) (Nantes).
- El Mrini, A., Maanan, M., Anthony, E.J., Taaouati, M., 2012a. An integrated approach to characterize the interaction between coastal morphodynamics, geomorphological setting and human interventions on the Mediterranean beaches of northwestern Morocco. *Appl. Geogr.* 35 (1), 334–344. <https://doi.org/10.1016/j.apgeog.2012.08.009>.
- El Mrini, A., Anthony, E.J., Maanan, M., Taaouati, M., Nachite, D., 2012b. Beach-dune degradation in a Mediterranean context of strong development pressures, and the missing integrated management perspective. *Ocean Coast Manag.* 69, 299–306. <https://doi.org/10.1016/j.ocecoaman.2012.08.004>.
- Estrada, F., Galindo-Zaldívar, J., Vázquez, J.T., Ercilla, G., D'Acremont, E., Alonso, B., Gorini, C., 2018. Tectonic indentation in the central Alboran Sea (westernmost Mediterranean). *Terra. Nova* 30 (1), 24–33. <https://doi.org/10.1111/ter.12304>.
- Estrada, F., González-Vida, J.M., Peláez, J.A., Galindo-Zaldívar, J., Ortega, S., Macías, J., Vázquez, J.T., Ercilla, G., 2021. Tsunami generation potential of a strike-slip fault tip in the westernmost Mediterranean. *Sci. Rep.* 11 (1), 16253. <https://doi.org/10.1038/s41598-021-95729-6>.
- Fajri, Z., Outisk, M., Khouyaoui, Y., El Moussaoui, S., El Talibi, H., Aboumaria, K., 2021. Numerical simulation of tsunami hazards in south Atlantic coast: case of the city of Agadir - Morocco: preliminary result. *ISPRS - Int. Arch. Photogramm. Remote Sens. Spat. Inf. Sci.* 46W5, 219–223. <https://doi.org/10.5194/isprs-archives-XLVI-4-W5-2021-219-2021>.
- French Ministry of the Environment, Energy and the Sea (MEEM), 2016. National Flood Vulnerability Framework, Guide Resulting from the Work of the Vulnerability Reference Framework WG Co-piloted by CEPRI and DGPR Work Carried Out by Cerema. http://www.developpement-durable.gouv.fr/sites/default/files/20160923_Guide_GT_Referentiel_vulnerabilite.pdf.
- Fukui, N., Prasetyo, A., Mori, N., 2019. Numerical modeling of tsunami inundation using upscaled urban roughness parameterization. *Coast. Eng.* 152, 103534. <https://doi.org/10.1016/j.coastaleng.2019.103534>.
- Gayer, G., Leschka, S., Nöhren, I., Larsen, O., Günther, H., 2010. Tsunami inundation modelling based on detailed roughness maps of densely populated areas. *Nat. Hazards Earth Syst. Sci.* 10 (8), 1679–1687. <https://doi.org/10.5194/nhess-10-1679-2010>.
- GEBCO Bathymetric Compilation Group 2021, 2021. The GEBCO_2021 Grid - a Continuous Terrain Model of the Global Oceans and Land. <https://doi.org/10.5285/C6612CBE-50B3-OCFF-E053-6C86ABC09F8F>.
- Geertsema, M., Highland, L.M., 2011. Landslides: human health effects. In: Nriagu, J.O. (Ed.), *Encyclopedia of Environmental Health*. Elsevier, Burlington, pp. 380–395. <https://doi.org/10.1016/B978-0-444-52272-6.00550-X>.
- González, M., Medina, R., 1998. Probabilistic model for tsunami-wave elevation along the Alboran seacoast. *Coast. Eng. Proc.* 1168–1181. <https://doi.org/10.9753/icce.v26.6.p>.
- González, F.I., Titov, V.V., Mofjeld, H.O., Venturato, A.J., Simmons, R.S., Hansen, R., Combellic, R., Eisner, R.K., Hoirup, D.F., Yanagi, B.S., Yong, S., Darienzo, M., Priest, G.R., Crawford, G.L., Walsh, T.J., 2005. Progress in NTHMP hazard assessment. *Nat. Hazards* 35 (1), 89–110. <https://doi.org/10.1007/s11069-004-2406-0>.
- González, M., Medina, R., Olabarrieta, M., Otero, L., Canales, C., 2010. Tsunami hazard assessment on the southern coast of Spain. *Turk. J. Earth Sci.* 19, 351–366. <https://doi.org/10.3906/yer-0812-8>.
- Goto, K., Chagué-Goff, C., Fujino, S., Goff, J., Jaffe, B., Nishimura, Y., Richmond, B., Sugawara, D., Szczuciński, W., Tappin, D.R., Witter, R.C., Yulianto, E., 2011. New insights of tsunami hazard from the 2011 Tohoku-oki event. *Mar. Geol.* 290 (1), 46–50. <https://doi.org/10.1016/j.margeo.2011.10.004>.
- Gràcia, E., Grevemeyer, I., Bartolomé, R., Perea, H., Martínez-Loriente, S., Gómez de la Peña, L., Villaseñor, A., Klinger, Y., Lo Iacono, C., Diez, S., Calahorra, A., Camafort, M., Costa, S., d'Acremont, E., Rabaute, A., Ranero, C.R., 2019. Earthquake crisis unveils the growth of an incipient continental fault system. *Nat. Commun.* 10 (1), 3482. <https://doi.org/10.1038/s41467-019-11064-5>.
- Grevemeyer, I., Gràcia, E., Villaseñor, A., Leuchters, W., Watts, A.B., 2015. Seismicity and active tectonics in the Alboran Sea, Western Mediterranean: constraints from an offshore-onshore seismological network and swath bathymetry data. *J. Geophys. Res. Solid Earth* 120 (12), 8348–8365. <https://doi.org/10.1002/2015JB012073>.
- Griffin, J., Latief, H., Kongko, W., Harig, S., Horspool, N., Hanung, R., Rojali, A., Maher, N., Fuchs, A., Hossen, J., Upi, S., Edi, D., Rakowsky, N., Cummins, P., 2015. An evaluation of onshore digital elevation models for modeling tsunami inundation zones. *Front. Earth Sci.* 3. <https://doi.org/10.3389/feart.2015.00032>.
- Hampton, M.A., Lee, H.J., Locat, J., 1996. Submarine landslides. *Rev. Geophys.* 34 (1), 33–59. <https://doi.org/10.1029/95RG03287>.
- Harbitz, C., Løvholt, F., Pedersen, G., Masson, D., 2006. Mechanisms of tsunami generation by submarine landslides: a short review. *Nor. Geol. Tidsskr.* 86, 255–264.
- Harbitz, C.B., Løvholt, F., Bungum, H., 2014. Submarine landslide tsunamis: how extreme and how likely? *Nat. Hazards* 72 (3), 1341–1374. <https://doi.org/10.1007/s11069-013-0681-3>.
- Haut Commissariat au Plan, 2014. Recensement général de la population et de l'habitat 2014 [WWW Document]. URL. <https://rgph2014.hcp.ma/>, 9.30.21.
- Juan, C., Ercilla, G., Javier Hernández-Molina, F., Estrada, F., Alonso, B., Casas, D., García, M., Farran, M., Llave, E., Palomino, D., Vázquez, J.-T., Medialdea, T., Gorini, C., D'Acremont, E., El Moumni, B., Ammar, A., 2016. Seismic evidence of current-controlled sedimentation in the Alboran Sea during the pliocene and quaternary: palaeoceanographic implications. *Mar. Geol. Contourite Log-Book: Significance Palaeoceanogr. Ecosyst. Slope Instabil.* 378, 292–311. <https://doi.org/10.1016/j.margeo.2016.01.006>.
- Kaiser, G., Scheele, L., Kortenhaus, A., Løvholt, F., Römer, H., Leschka, S., 2011. The influence of land cover roughness on the results of high-resolution tsunami inundation modeling. *Nat. Hazards Earth Syst. Sci.* 11 (9), 2521–2540. <https://doi.org/10.5194/nhess-11-2521-2011>.

- Karrouchi, M., Touhami, M.O., Oujidi, M., Chourak, M., 2016. Mapping of flooding risk areas in the Tangier-Tetouan region: case of Martil watershed (northern Morocco). *Int. J. Res. Sci. Innov. Appl. Stud.* 14 (4), 1019–1035.
- Leone, F., Baptista, M., Zourarah, B., Khalid, M., Lavigne, F., Meschinet, N., Omira, R., Mellas, S., Péroche, M., Lagahé, É., H. A., G. M., Grancher, D., Cherel, J.-P., Sahal, A., Denain, J.-C.N., Meunier, D.I., 2012. Evaluation des vulnérabilités territoriales et humaines face aux tsunamis au Maroc (façade atlantique et ville d'El Jadida) : données historiques, modélisation de l'aléa et des enjeux humains, critères de vulnérabilité, indicateurs de risque, aide à la gestion des évacuations, p. 190.
- Liew, S.C., Gupta, A., Wong, P.P., Kwok, L.K., 2010. Recovery from a large tsunami mapped over time: the Aceh coast, Sumatra. *Geomorphology* 114 (4), 520–529. <https://doi.org/10.1016/j.geomorph.2009.08.010>.
- Løvholt, F., Setiadi, N.J., Birkmann, J., Harbitz, C.B., Bach, C., Fernando, N., Kaiser, G., Nadim, F., 2014. Tsunami risk reduction – are we better prepared today than in 2004? *Int. J. Disaster Risk Reduc.* 10, 127–142. <https://doi.org/10.1016/j.ijdrr.2014.07.008>.
- Lynett, P.J., 2016. Precise prediction of coastal and overland flow dynamics: a grand challenge or a fool's errand. *J. Disaster Res.* 11 (4), 615–623. <https://doi.org/10.20965/jdr.2016.p0615>.
- Macías, J., Vázquez, J.T., Fernández-Salas, L.M., González-Vida, J.M., Bárcenas, P., Castro, M.J., Díaz-del-Río, V., Alonso, B., 2015. The Al-Borani submarine landslide and associated tsunami. A modelling approach. *Mar. Geol.* 361, 79–95. <https://doi.org/10.1016/j.margeo.2014.12.006>.
- Mangeny, A., Bouchut, F., Thomas, N., Vilotte, J.P., Bristeau, M.O., 2007. Numerical modeling of self-channeling granular flows and of their levee-channel deposits. *J. Geophys. Res. Earth Surf.* 112 (F02). <https://doi.org/10.1029/2006JF000469>.
- Marras, S., Mandli, K.T., 2021. Modeling and simulation of tsunami impact: a short review of recent advances and future challenges. *Geosci.* 11 (1), 5. <https://doi.org/10.3390/geosciences11010005>.
- Mellas, S., Leone, F., Omira, R., Gherardi, M., Baptista, M.-A., Zourarah, B., Péroche, M., Lagahé, É., 2012. Le risque tsunamique au Maroc : modélisation et évaluation au moyen d'un premier jeu d'indicateurs d'exposition du littoral atlantique. *Phys. Géogr. Géogr. Phys. Environ.* 6, 119–139. <https://doi.org/10.4000/physio-geo.2589>.
- Ministry of Civil Defence & Emergency Management, 2016. *Tsunami Evacuation Zones - Director's Guideline for Civil Defence Emergency Management Groups*. Wellington, New-Zealand [DGL 08/16].
- Ministry of Land, Infrastructure, Transport and Tourism, 2012. *Guide to Determining the Potential Tsunami Inundation*. Seacoast Office, Water and Disaster Management Bureau, Ministry of Land, Infrastructure, Transport and Tourism and Coast Division. River Department, National Institute for Land and Infrastructure Management, Ministry of Land, Infrastructure, Transport and Tourism, Tokyo, Japan.
- National Geophysical Data Center/World Data Service: NCEI/WDS. n.d. Global Historical Tsunami Database. NOAA National Centers for Environmental Information. <https://doi.org/10.7289/V5PN93H7> (accessed 1.February.2023).
- National Office of Airports, 2023. *Travaux de construction d'un nouveau terminal, une nouvelle tour de contrôle et aménagements extérieur à l'aéroport de Tétouan/Saniat R'mel*. (No. N° 031-23-AOO).
- OECD, 2016. *Étude de l'OCDE sur la gestion des risques au Maroc*. Organisation for Economic Co-operation and Development, Paris. <https://doi.org/10.1787/9789264267145-fr>.
- Omira, R., Baptista, M.A., Miranda, J.M., Toto, E., Catita, C., Catalão, J., 2010. Tsunami vulnerability assessment of Casablanca-Morocco using numerical modelling and GIS tools. *Nat. Hazards* 54 (1), 75–95. <https://doi.org/10.1007/s11069-009-9454-4>.
- Omira, R., Baptista, M.A., Mellas, S., Leone, F., Meschinet de Richemond, N., Zourarah, B., Cherel, J.-P., 2012. The November, 1st, 1755 tsunami in Morocco: can numerical modeling clarify the uncertainties of historical reports? In: Lopez, Gloria I. (Ed.), *Tsunami - Analysis of a Hazard*. IntechOpen, Rijeka, pp. 61–75. <https://doi.org/10.5772/51864>.
- Omira, R., Baptista, M.A., Matias, L., 2015. Probabilistic tsunami hazard in the Northeast Atlantic from near- and far-field tectonic sources. *Pure Appl. Geophys.* 172 (3–4), 901–920. <https://doi.org/10.1007/s00024-014-0949-x>.
- Papadopoulos, G., 2016. Introduction. In: Papadopoulos, G. (Ed.), *Tsunamis in the European-Mediterranean Region*. Elsevier, Boston, pp. 15–17. <https://doi.org/10.1016/B978-0-12-420224-5.00015-6>.
- Papadopoulos, G.A., Fokaefs, A., 2013. Near-field tsunami early warning and emergency planning in the Mediterranean Sea. *Res. Geophys.* 3 (4), 24–31. <https://doi.org/10.4081/rg.2013.e4>.
- Paris Region Institute, 2020. *Schéma Directeur d'Aménagement Urbain du Grand Tétouan - Phase 2 : Stratégies d'Aménagement et de Développement et carte du SDAU* (Paris, France).
- Peruzzetto, M., 2021. *Numerical Modeling of Dry and Water-Laden Gravitational Flows for Quantitative Hazard Assessment* (PhD Thesis). Université Paris Cité.
- Ramalho, I., Omira, R., El Moussaoui, S., Baptista, M.A., Zaghoul, M.N., 2018. Tsunami-induced morphological change – a model-based impact assessment of the 1755 tsunami in NE Atlantic from the Morocco coast. *Geomorphology* 319, 78–91. <https://doi.org/10.1016/j.geomorph.2018.07.013>.
- Raymond, C., Horton, R.M., Zscheischler, J., Martius, O., AghaKouchak, A., Balch, J., Bowen, S.G., Camargo, S.J., Hess, J., Kornhuber, K., Oppenheimer, M., Ruane, A.C., Wahl, T., White, K., 2020. Understanding and managing connected extreme events. *Nat. Clim. Change* 10 (7), 611–621. <https://doi.org/10.1038/s41558-020-0790-4>.
- Renou, C., Lesne, O., Mangin, A., Rouffi, F., Atillah, A., El Hadani, D., Moudni, H., 2011. Tsunami hazard assessment in the coastal area of Rabat and Salé, Morocco. *Nat. Hazards Earth Syst. Sci.* 11 (8), 2181–2191. <https://doi.org/10.5194/nhess-11-2181-2011>.
- Röbke, B.R., Vött, A., 2017. The tsunami phenomenon. *Prog. Oceanogr.* 159, 296–322. <https://doi.org/10.1016/j.poccean.2017.09.003>.
- Rodriguez, M., Maleuvre, C., Jollivet-Castelot, M., d'Acromont, E., Rabaute, A., Lafosse, M., Ercilla, G., Vázquez, J.-T., Alonso, B., Ammar, A., Gorini, C., 2017. Tsunamiogenic submarine landslides along the Xauen-Tofiño banks in the Alboran Sea (western Mediterranean Sea). *Geophys. J. Int.* 209 (1), 266–281. <https://doi.org/10.1093/gji/ggx028>.
- Sadegh, M., Moftakhari, H., Gupta, H.V., Ragno, E., Mazdiyasn, O., Sanders, B., Matthew, R., AghaKouchak, A., 2018. Multihazard scenarios for analysis of compound extreme events. *Geophys. Res. Lett.* 45 (11), 5470–5480. <https://doi.org/10.1029/2018GL077317>.
- Sadeh, Y., Cohen, H., Maman, S., Blumberg, D., 2018. Evaluation of Manning's n roughness coefficient in arid environments by using SAR backscatter. *Rem. Sens.* 10 (10), 1505. <https://doi.org/10.3390/rs10101505>.
- Sahal, A., 2011. *Le risque tsunami en France : contributions méthodologiques pour une évaluation intégrée par scénarios de risque*. (PhD Thesis). Université Panthéon-Sorbonne - Paris I.
- Sharma, A.S. (Ed.), 2012. *Extreme Events and Natural Hazards: the Complexity Perspective*. Geophysical monograph. American Geophysical Union, Washington, DC, p. 371.
- Sorensen, R.M., 2006. *Basic Coastal Engineering*, third ed. Springer, New York. <https://doi.org/10.1007/b101261>.
- Sugawara, D., 2021. Numerical modeling of tsunami: advances and future challenges after the 2011 Tohoku earthquake and tsunami. *Earth Sci. Rev.* 214, 103498. <https://doi.org/10.1016/j.earscirev.2020.103498>.
- Suppasri, A., Leelawat, N., Latcharote, P., Roeber, V., Yamashita, K., Hayashi, A., Ohira, H., Fukui, K., Hisamatsu, A., Nguyen, D., Imamura, F., 2017. The 2016 Fukushima earthquake and tsunami: local tsunami behavior and recommendations for tsunami disaster risk reduction. *Int. J. Disaster Risk Reduc.* 21, 323–330. <https://doi.org/10.1016/j.ijdrr.2016.12.016>.
- Synolakis, C.E., Bernard, E.N., Titov, V.V., Kanoğlu, U., González, F.I., 2008. Validation and verification of tsunami numerical models. *Pure Appl. Geophys.* 165 (11), 2197–2228. <https://doi.org/10.1007/s00024-004-0427-y>.
- Tadibaght, A., Kamal, A., Bounab, A., El M'rini, A., Siame, L., El Kharim, Y., Bellier, O., el Ouaty, O., 2022a. Quantitative risk assessment in El-Jadida (Northern Atlantic Coast of Morocco) for a tsunami scenario equivalent to that of the 1755 Lisbon earthquake. *Environ. Earth Sci.* 81. <https://doi.org/10.1007/s12665-022-10277-0>.
- Tadibaght, A., El M'rini, A., Siame, L., Bellier, O., 2022b. Tsunami impact assessment for low-lying cities along the Northern Atlantic coast of Morocco using MIRONE software. *J. Afr. Earth Sci.* 104580. <https://doi.org/10.1016/j.jafrearsci.2022.104580>.
- Taher, M., Mourabit, T., Talibi, H.E., Etebaai, I., Bourjila, A., Errahmouni, A., Lamghar-baj, M., 2022. The risk mapping of coastal flooding areas due to tsunami wave run-up using DAS model and its impact on Nekor bay (Morocco). *Ecol. Eng. Environ. Technol.* 23 (4), 136–148. <https://doi.org/10.12912/27197050/150310>.
- Tappin, D.R., Watts, P., Grilli, S.T., 2008. The Papua New Guinea tsunami of 17 July 1998: anatomy of a catastrophic event. *Nat. Hazards Earth Syst. Sci.* 8 (2), 243–266. <https://doi.org/10.5194/nhess-8-243-2008>.
- Theilen-Willige, B., Löwner, R., Bchari, F.E., Malek, H.A., Chaibi, M., Charif, A., Nakhcha, C., Ougougdal, M.A., Ridaoui, M., Boumaggard, E., 2014. Remote sensing and GIS contribution to the detection of areas susceptible to natural hazards in the Safi area, W-Morocco. In: 2014 1st International Conference on Information and Communication Technologies for Disaster Management (ICT-DM). Presented at the 2014 1st International Conference on Information and Communication Technologies for Disaster Management. (ICT-DM), pp. 1–5. <https://doi.org/10.1109/ICT-DM.2014.6917786>.
- Tonini, R., Di Manna, P., Lorito, S., Selva, J., Volpe, M., Romano, F., Basili, R., Brizuela, B., Castro, M.J., de la Asunción, M., Di Bucci, D., Dolce, M., Garcia, A., Gibbons, S.J., Glimsdal, S., González-Vida, J.M., Løvholt, F., Macías, J., Piatanesi, A., Pizzimenti, L., Sánchez-Linares, C., Vittori, E., 2021. Testing tsunami inundation maps for evacuation planning in Italy. *Front. Earth Sci.* 9.
- Tsuji, Y., Yanuma, T., Murata, I., Fujiwara, C., 1991. Tsunami ascending in rivers as an undular bore. *Nat. Hazards* 4 (2), 257–266. <https://doi.org/10.1007/BF00162791>.
- Tufekci-Enginar, D., Dogan, G.G., Suzen, M.L., Yalciner, A.C., 2022. Performance analysis of open-source DEMs in tsunami inundation modelling. *Earth. Sci. Inform.* 15 (4), 2447–2466. <https://doi.org/10.1007/s12145-022-00852-1>.
- UNESCO/IOC, 2020. *Preparing for Community Tsunami Evacuations: from Inundation to Evacuation Maps, Response Plans and Exercises* (No. 82), Manuals and Guides. UNESCO, Paris, France.
- US National Tsunami Hazard Mitigation Program, 2021. *Part III: Tsunami Inundation Determination for Non-modeled Regions1, Tsunami Modeling and Mapping: Guidelines and Best Practices*. National Tsunami Hazard Mitigation Program Mapping and Modeling Subcommittee.
- World Bank, 2014. *Renforcement de la résilience du Maroc : Apports pour une stratégie de gestion intégrée des risques* (License: CC BY 3.0 IGO (Washington, DC)).
- Yamanaka, Y., Shimozono, T., 2022. Tsunami inundation characteristics along the Japan Sea coastline: effect of dunes, breakwaters, and rivers. *Earth Planets Space* 74 (1), 19. <https://doi.org/10.1186/s40623-022-01579-5>.